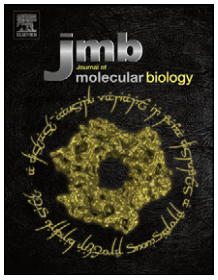

Generation of Fluorogen-Activating Designed Ankyrin Repeat Proteins (FADAs) as Versatile Sensor Tools

Marco Schütz [1], Alexander Batyuk [1], Christoph Klenk [1], Lutz Kummer [1], Seymour de Picciotto [2], Basri Gülbakan [3], Yufan Wu [1], Gregory A. Newby [1], Franziska Zosel [1], Jendrik Schöppe [1], Erik Sedlák [1], Peer R.E. Mittl [1], Renato Zenobi [3], K. Dane Wittrup [2] and Andreas Plückthun [1]

*1 - **Department of Biochemistry,** University of Zurich, CH-8057, Zurich, Switzerland*
*2 - **Koch Institute for Integrative Cancer Research,** Massachusetts Institute of Technology, Cambridge, MA 02139, USA*
*3 - **Department of Chemistry and Applied Biosciences,** ETH Zurich, CH-8093, Zurich, Switzerland*

Correspondence to Andreas Plückthun: *plueckthun@bioc.uzh.ch*
http://dx.doi.org/10.1016/j.jmb.2016.01.017
Edited by S. Koide

Abstract

Fluorescent probes constitute a valuable toolbox to address a variety of biological questions and they have become irreplaceable for imaging methods. Commonly, such probes consist of fluorescent proteins or small organic fluorophores coupled to biological molecules of interest. Recently, a novel class of fluorescence-based probes, fluorogen-activating proteins (FAPs), has been reported. These binding proteins are based on antibody single-chain variable fragments and activate fluorogenic dyes, which only become fluorescent upon activation and do not fluoresce when free in solution. Here we present a novel class of fluorogen activators, termed FADAs, based on the very robust designed ankyrin repeat protein scaffold, which also readily folds in the reducing environment of the cytoplasm. The FADA generated in this study was obtained by combined selections with ribosome display and yeast surface display. It enhances the fluorescence of malachite green (MG) dyes by a factor of more than 11,000 and thus activates MG to a similar extent as FAPs based on single-chain variable fragments. As shown by structure determination and *in vitro* measurements, this FADA was evolved to form a homodimer for the activation of MG dyes. Exploiting the favorable properties of the designed ankyrin repeat protein scaffold, we created a FADA biosensor suitable for imaging of proteins on the cell surface, as well as in the cytosol. Moreover, based on the requirement of dimerization for strong fluorogen activation, a prototype FADA biosensor for *in situ* detection of a target protein and protein–protein interactions was developed. Therefore, FADAs are versatile fluorescent probes that are easily produced and suitable for diverse applications and thus extend the FAP technology.

Introduction

The ability to image molecules in live cells has tremendously advanced molecular cell biology, as it allows for specific investigation of localization, trafficking, interactions, and functionality of single or multiple biological molecules *in vivo*. Fluorescent probes should be well detectable, exhibit low background signal, allow multiplex labeling with different fluorophores, show no cell toxicity, and minimize interference with cellular processes. Traditionally, fluorescent probes have been generated by genetic fusions of auto-fluorescent proteins to proteins of interest, which allows live-cell imaging. As a second strategy, a variety of fluorescent labeling methods, based on specific chemical or enzymatic coupling of fluorophores *via* a reactive moiety, have been established [1–5]. While chemically coupled conjugates extend the observable parameters over auto-fluorescent proteins, cells generally need to be permeabilized for taking up the conjugate, limiting their use on undisturbed live cells or surface proteins.

More recently, another class of fluorescent probes, so-called fluorogen-activating proteins (FAPs), has been reported [6]. FAPs have so far been antibody single-chain variable fragments (scFvs) that specifically bind and activate fluorogenic dyes. These dyes are almost non-fluorescent when free in solution. However, upon activation by a binding molecule, they strongly fluoresce. To date, several FAPs that activate different fluorogenic dyes have been generated by selection with yeast surface display and were successfully applied in multiple imaging applications [6–14]. However, despite the proven usability of these FAPs, the technology has some intrinsic limitations due to the antibody nature of these molecules. For instance, they rely on intramolecular disulfide bonds for structural integrity and activity, and many scFvs have only moderate stability and tend to aggregate, especially as fusion proteins (reviewed in Ref. [15]).

Therefore, we aimed to expand the FAP technology with another class of binding proteins with properties superior to those of most scFvs. Designed ankyrin repeat proteins (DARPins), which are engineered non-immunoglobulin scaffold proteins not containing any cysteines and further characterized by high solubility, stability, and production yields, are ideal candidates for that purpose [16–18]. DARPins are composed of N- and C-terminal capping repeats with a variable number of stackable internal repeat modules in between. Next to fixed framework positions, DARPins have randomized positions that create a large potential interaction surface presented on the rigid scaffold. Thus, selections from combinatorial DARPin libraries allow the generation of DARPins binding a wide variety of different targets with high affinity and specificity [19–30].

Here we present the generation of fluorescence-activating DARPins (FADAs) by combining ribosome display selections with yeast surface display maturation. The FADA obtained in this study, termed FADA-3210, enhances the fluorescence of fluorogenic malachite green (MG) dyes by up to a factor of 11,100. The crystal structure of FADA-3210 in complex with a MG dye, as well as *in vitro* experiments with purified protein, revealed that FADA-3210 was evolved to form a homodimer in order to achieve such a strong activation of the MG dyes. We demonstrate that FADA-3210 could be used as a versatile marker for labeling of intracellular and extracellular proteins. We then generated a prototype biosensor that reports on the *in situ* concentration of a target protein, based on competition between dimerization-dependent fluorogen activation and binding of a secondary target. This might be extended to detect protein–protein interaction dynamics. Due to the beneficial properties of DARPins, FADAs represent a valuable extension of the FAP technology toolbox.

Results

Ribosome display followed by yeast surface display selections lead to a DARPin with strong fluorescence activation of MG dyes

We used combinatorial DARPin libraries for the selection of MG-binding DARPins by ribosome display [16,31]. For this purpose, the fluorogen target was immobilized in biotinylated form, MG-11p-biotin, to perform ribosome display selections with the N2C (two internal repeats) and the N3C (three internal repeats) DARPin libraries. All MG dyes used in this study are summarized in Fig. S1. While no enrichment of binders was obtained from the N2C library, the selections with the N3C library resulted in a pool of MG-binding DARPins. Because we expected the affinity of the DARPins for the binding of this small dye molecule to be rather low, the selected DARPin pool was further subjected to ribosome display off-rate selections [32]. From these selections, we isolated two dominant MG-binding DARPins, termed FADA-C1 and FADA-D4. However, even though both of these DARPins bind MG derivatives, they only exhibit weak fluorogen activation properties (Figs. 1 and 2).

While ribosome display is very well suited to select for high-affinity binding, no selection pressure on fluorescence activation can be applied. Thus, the weak fluorogen activation of the DARPins obtained from the ribosome display selections is the consequence of selection pressure applied only on fluorogen binding, but not on fluorogen activation. In contrast, selection pressure on fluorescence activation can be easily exerted by using yeast surface display, which involves the selection of the desired phenotype based on a fluorescence readout with fluorescence-activated cell sorting (FACS) [33–36].

Therefore, we used yeast surface display to mature the binders obtained from the ribosome display selections, FADA-C1 and FADA-D4, toward stronger fluorogen activation of the MG derivative MG-2p (Fig. S1). First, a library was created by randomization of FADA-C1 and FADA-D4 with mutagenic PCR. This library was then subjected to selections with yeast surface display, in which the clones with the highest fluorescence intensity upon addition of MG-2p were isolated in two rounds of FACS, thus enriching for the strongest MG-2p fluorescence activators. This maturation selection was performed for three rounds, each round including a randomization step followed by two selections with FACS. Indeed, the resulting pool of matured DARPins, termed FADA 3.2, showed a significant increase of fluorescence activation of MG-2p compared to FADA-C1 and FADA-D4 (Fig. 1).

From the FADA 3.2 pool, we isolated a dominant FADA, termed FADA-3210, which is a descendant of

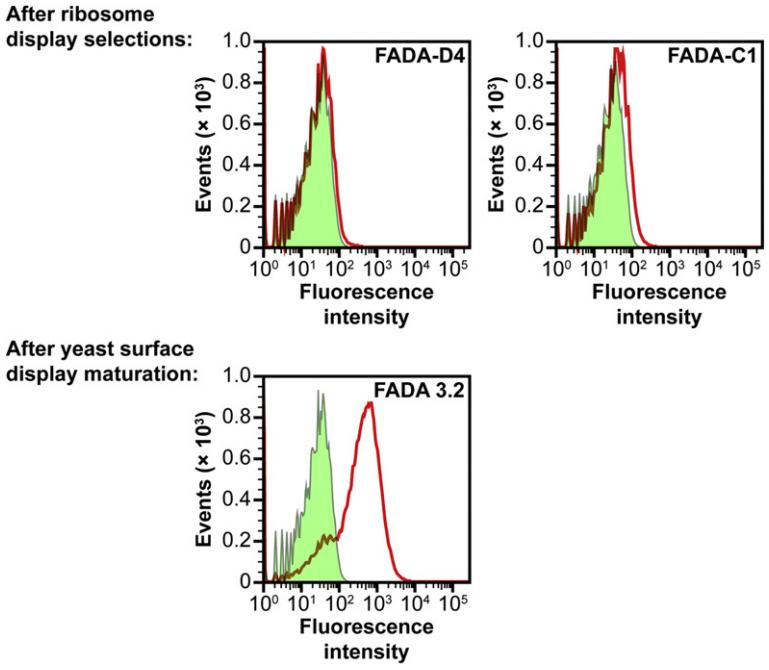

Fig. 1. Fluorogen-activating DARPins (FADAs) matured by selections with yeast surface display. Flow cytometry histogram plots of yeast cells displaying FADAs are shown. The cells were measured either without addition of fluorogenic dye (background, tinted green-filled curves) or with 10 nM MG-2p (red curves). For the FADAs initially obtained from ribosome display selections (FADA-D4 and FADA-C1, top panel), the measured fluorescence activation is very weak. In contrast, the selected pool of FADAs after three rounds of maturation with yeast surface display selecting for fluorescence directly (FADA 3.2, bottom panel) shows a strong signal for fluorescence activation. For each sample, 50,000 events were recorded and identical acquisition settings were used in order to allow comparative analysis.

FADA-C1. Interestingly, FADA-3210 contains only five additional mutations compared to FADA-C1 (Fig. S2). FADA-C1 and FADA-3210 were expressed and purified, and fluorogen activation of MG-2p and of its cell-permeable derivative MG-ester (Fig. S1) was measured in solution (Fig. 2a). While FADA-C1 shows an enhancement of fluorescence by a factor of approximately 130–180 compared to background, the fluorescence activation of MG-2p and MG-ester by FADA-3210 was much stronger with a factor of approximately 11,100 and 7400, respectively. The fluorogen activation of FADA-3210 is thus similar to the activation obtained with MG-activating scFvs previously described by Waggoner and co-workers [6]. Additionally, the fluorescence spectrum obtained from MG-2p activated by FADA-3210 has an excitation maximum at approximately 625 nm and an emission maximum at approximately 650 nm (Fig. 2b), which is very similar to that of scFv-activated MG-2p [6].

The crystal structure of the FADA-3210/MG-2p complex reveals that MG-2p is bound by two DARPin molecules forming a homodimer

In order to get more insights into the mechanism of MG-2p fluorescence activation and to investigate how the additional mutations in FADA-3210 contribute to this effect, we set up co-crystallization experiments of FADA-3210 in complex with MG-2p and determined the structure of this complex by X-ray crystallography at 2.6 Å resolution. Interestingly, we found that MG-2p is bound by two FADA-3210 DARPins that form a homodimer. The complex has *C*2 symmetry with the symmetry axis passing through the central carbon atom of MG-2p along the bond to the phenyl group, such that the corresponding N- and C-termini of each protomer are pointing to the same direction (Fig. 3).

While the MG moiety of MG-2p shows well-defined electron density (Figs. S3 and S4), it was not possible to model the complete 2p chain of MG-2p. However, the weak electron density obtained in this region suggests that MG-2p is bound in two conformations in which the 2p chain can be accommodated in opposing directions within the FADA-3210 dimer (Fig. S3).

MG-2p is bound in the C-terminal part of the DARPin homodimer, where the residues from the third internal repeat, as well as from the C-capping repeat, make contacts to the dye and hold the triarylmethane moiety of MG-2p in a right-handed propeller conformation. This conformation is very similar to the conformation calculated as the electronic ground state of the unbound dye [37] (Fig. S4). A similar propeller form of MG is also found in an RNA aptamer [38] (PDB ID: 1q8n), in an immunoglobulin lambda variable domain dimer [39] (PDB ID: 4k3h), and in complexes of MG bound to multidrug binding proteins (PDB IDs: 3hti, 3bqz, 3br0, 3btc, 3btl, and 1jup). This suggests that the binding molecules have been selected to bind a conformation of the ligand that is highly populated, namely, a propeller conformation close to the ground state.

The fluorescence enhancement thus requires that MG-2p is held rather rigidly in its ground-state conformation in a tight fitting hydrophobic pocket. Except for the asparagine N^{156}, this hydrophobic

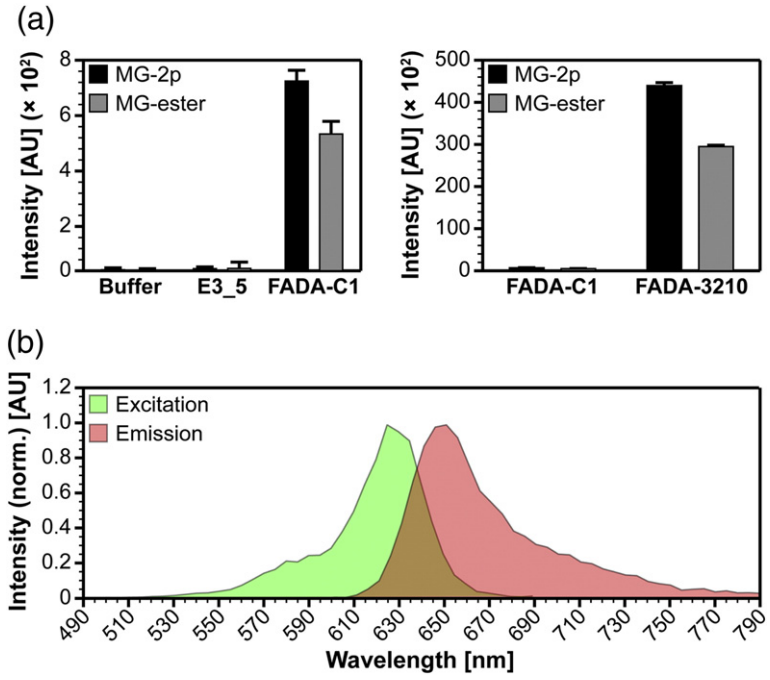

Fig. 2. Fluorescence activation of purified FADAs in solution. (a) Fluorogen activation of MG-2p (black bars) and MG-ester (gray bars) with purified DARPins in solution are shown. DARPins (2 μM) were incubated with 200 nM MG-2p or 200 nM MG-ester. As a background control, samples without DARPin (buffer) or with a non-selected N3C DARPin (E3_5) were included. Note the different *y*-axes in both plots. Compared to the background, FADA-C1 (obtained from ribosome display selections) shows an enhancement of fluorescence of MG-2p and MG-ester by a factor of approximately 180 and 130, respectively. Much stronger fluorogen activation is achieved with FADA-3210 (obtained from yeast surface display maturation), which enhances the fluorescence of MG-2p and MG-ester by a factor of approximately 11,100 and 7400, respectively. Error bars indicate standard deviations from triplicates. (b) Shown are the excitation (green, tinted) and the emission spectra (red, tinted) of MG-2p activated by FADA-3210. Purified FADA-3210 (1 μM) was incubated with 200 nM MG-2p for recording of the spectra. The excitation maximum of MG-2p activated by FADA-3210 is at approximately 625 nm with an emission maximum at approximately 650 nm. The data of each spectrum were normalized to the maximum signal intensity, set to 1.0.

binding pocket consists of aromatic residues (W^{114}, Y^{122}, F^{123}, and F^{145}) that hold MG-2p in its conformation by a symmetric arrangement *via* T-shaped π-stacking interactions (W^{114}) and van der Waals contacts (Fig. 4). Interestingly, all of these residues are present in FADA-C1 as well, indicating that the ligand-binding site remained unaltered during maturation.

Indeed, the analysis of residues involved in the dimer formation and in ligand contacts (Table 1) suggests that the additional mutations in FADA-3210 are stabilizing the dimeric state of the DARPin rather than creating new binding contacts to MG-2p. An extended dimerization interface is present both in FADA-C1 and in the evolved FADA-3210, comprising the arginine R^{46} side chain, sandwiched between the parallel tyrosine Y^{57} and tryptophan W^{90} side chains (Fig. 5). However, three out of the five additional mutations in FADA-3210 are involved in additional dimerization contacts (S^{45}, Y^{59}, and Y^{155}). From these residues, tyrosine Y^{155} appears to have the strongest effect and is involved in an extended dimerization interface with the residues tyrosine Y^{122} and lysine K^{147}, consisting of five intermolecular bonding interactions (Fig. 5). The K^{147} side chains form an intermolecular hydrogen bond to the Y^{155}

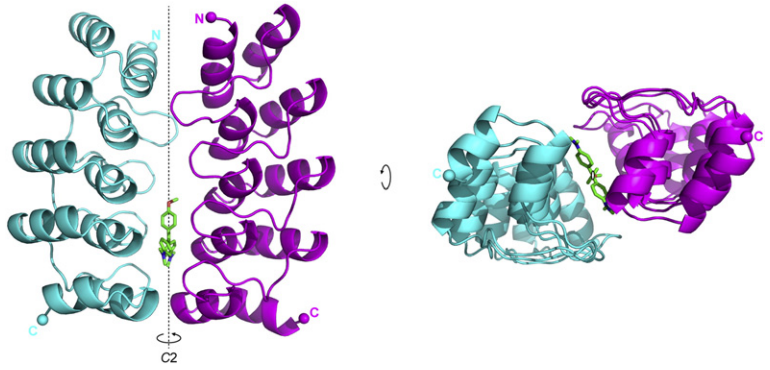

Fig. 3. Crystal structure of dimeric FADA-3210 binding one MG-2p molecule. The FADA-3210 homodimer (cyan and magenta cartoons) binding one MG-2p molecule (green sticks) is shown perpendicular to the 2-fold axis (left) and from the C-terminal ends of the DARPins along the 2-fold symmetry axis (right). The N- and C-termini of both FADA-3210 molecules forming the homodimer are pointing in the same direction (depicted as spheres and labeled with N and C, respectively). The complex shows an overall *C*2 symmetry with a symmetry axis that passes through the central carbon atom of MG-2p along the bond to the phenyl group. The *C*2 symmetry axis is depicted as a broken line (left) or as an ellipse (right). The R_2 moiety (as defined in Fig. S1) is not shown because it is weakly defined in the electron density (see Fig. S3).

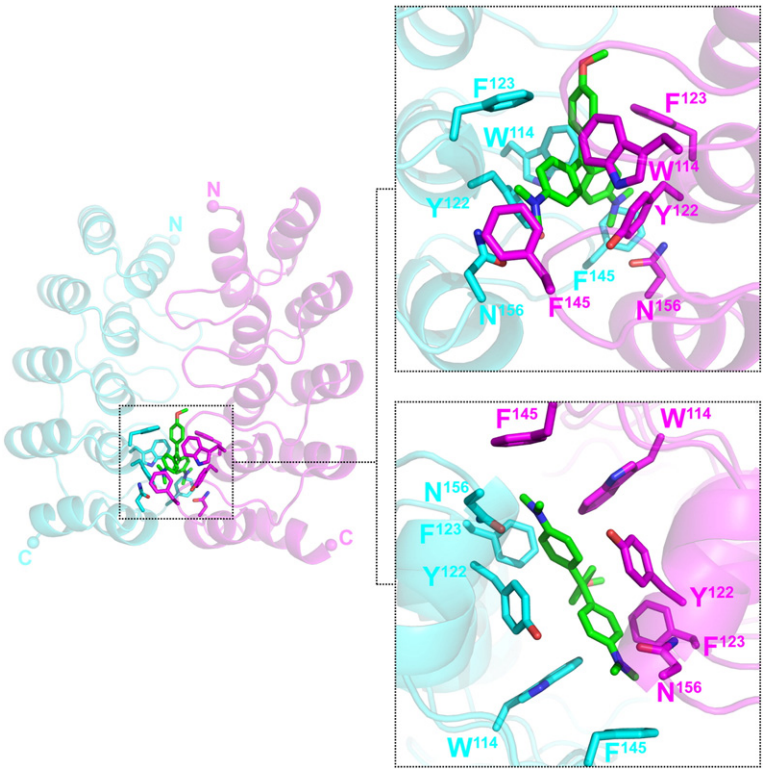

Fig. 4. MG-2p-binding site of the FADA-3210 dimer. Close-up views of the MG-2p-binding site in two perpendicular orientations are shown. Residues making contacts to the dye molecule were identified with LigPlot+ (v1.4.5) [60] and are shown as sticks. MG-2p is bound at the C-terminal part of the two DARPins by residues from the third internal repeat (W^{114}, Y^{122}, and F^{123}) and from the C-capping repeat (F^{145} and N^{156}). The hydrophobic binding site consists of pairwise symmetrical side chains, all being aromatic with the exception of N^{156}. The relative orientation of W^{114} to the dye allows T-shaped π-stacking, while all other residues make van der Waals contacts to the dye molecule.

backbone carbonyl group of the other dimer subunit. Additionally, the Y^{155} side chains of the two dimer subunits stack to each other allowing parallel π-interactions, while also being involved in intermolecular hydrogen bonds to the Y^{122} side chains of the other FADA-3210 molecule. Next to providing strong dimerization contacts, this network of interactions further forms a hydrophobic lid, which shields the dye from the solvent from the C-terminal end. Furthermore, the conformation of the MG-2p-binding Y^{122}

Table 1. Residues of FADA-3210 involved in dimerization or MG-2p binding

Residue	Position	Contact	Remark
Dimerization			
E^{20}	Framework	Hydrophobic (E^{20})	
R^{23}	Framework	Hydrophobic (R^{23})	
S^{45}	Randomized	Hydrophobic (Y^{57} and Y^{59})	N^{45} in FADA-C1
R^{46}	Randomized	Polar (D^{56}), hydrophobic (Y^{57} and W^{90})	
D^{56}	Randomized	Polar (R^{46})	
Y^{57}	Randomized	Hydrophobic (S^{45} and R^{46})	
Y^{59}	Framework (mutated)	Hydrophobic (S^{45})	H^{59} in FADA-C1
Y^{79}	Randomized	Hydrophobic (W^{90})	
W^{90}	Randomized	Hydrophobic (R^{46} and Y^{79})	
F^{112}	Randomized	Hydrophobic (F^{123})	
Y^{122}	Randomized	Polar (Y^{155})	
F^{123}	Randomized	Hydrophobic (F^{112})	
F^{145}	Framework	Hydrophobic (N^{156})	
K^{147}	Framework	Polar (Y^{155})	
I^{152}	Framework	Hydrophobic (Y^{155})	
Y^{155}	Framework (mutated)	Polar (Y^{122} and K^{147}), hydrophobic (I^{152})	D^{155} in FADA-C1
N^{156}	Framework	Hydrophobic (F^{145})	
MG-2p binding			
W^{114}	Randomized	Hydrophobic	
Y^{122}	Randomized	Hydrophobic	
F^{123}	Randomized	Hydrophobic	
F^{145}	Framework	Hydrophobic	
N^{156}	Framework	Hydrophobic	

Residues involved in dimerization or MG-2p binding were identified by using the program LigPlot+ (v1.4.5) [60].

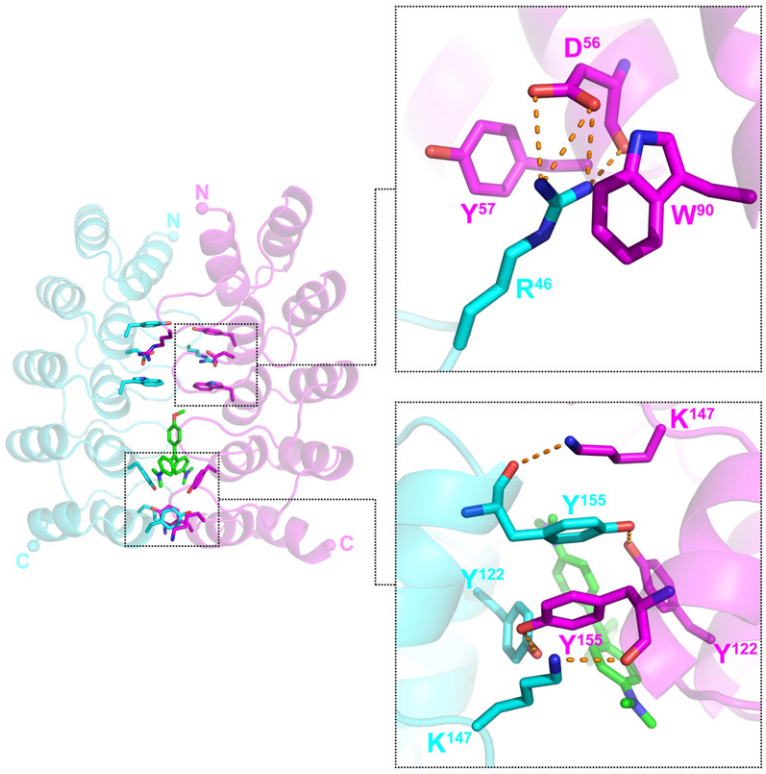

Fig. 5. Dimerization contacts between the two FADA-3210 molecules in the homodimer. Close-up views of the two major dimerization contacts are shown. The first dimerization interface (top) includes an arginine side chain (R^{46}) sandwiched between parallel oriented tyrosine and tryptophan side chains (Y^{57} and W^{90}). The R^{46} side chain forms hydrogen bonds to the carboxyl atoms of an aspartate side chain and backbone carbonyl (D^{56}), thereby being held in a parallel orientation with the Y^{57} and W^{90} side chains. Due to the symmetric arrangement of the homodimer, this interaction interface exists twice in the dimer. All of these residues are also present in FADA-C1 and thus may provide a dimerization site for the ancestor DARPin as well. The second major dimerization site (bottom) involves tyrosine Y^{122}, lysine K^{147}, and tyrosine Y^{155} at the C-terminal part of FADA-3210 close to the MG-2p-binding site. The symmetrical arrangement of this interaction site supports parallel π-stacking of the two Y^{155} side chains, which are also involved in intermolecular hydrogen bonds to the Y^{122} side chains of the other FADA-3210 molecule. An additional intermolecular hydrogen bond is formed between the side chain of K^{147} and the carbonyl group of the Y^{155} backbone. This well-defined interaction network shields the MG-2p molecule from the solvent by forming a hydrophobic lid at the C-terminal end of the DARPin and further stabilizes the conformation of Y^{122}, which also makes binding contacts to MG-2p. Y^{155} represents a strongly selected mutation in matured FADAs (D^{155} in FADA-C1). Thus, the generation of this extended dimerization interface may be the key evolutionary event in the maturation of FADA-C1, in which these interactions are not present.

residue is also stabilized by interaction across this dimerization interface. In contrast, FADA-C1 contains an aspartate instead of a tyrosine residue at position 155, which prevents formation of this interaction network.

Mass spectrometry confirms that a FADA-3210 homodimer binds one dye molecule

To independently examine the suggested binding stoichiometry in solution, we performed native nanoelectrospray ionization mass spectrometry (nanoESI-MS), which allows preservation of non-covalent protein–protein and protein–ligand interactions from solution [40,41]. FADA-3210 was incubated either without or with four different MG derivatives and analyzed by nanoESI-MS (Fig. 6). In each sample, the obtained mass spectra had a bimodal charge state distribution consisting of monomeric and dimeric charge states. At 5 μM FADA-3210, the dimeric species were clearly dominating. In the presence of MG derivatives, only FADA-3210 dimers were found to bind MG, with one dimer binding one dye molecule. In contrast, no monomer/dye complexes were observed.

To further confirm the dimeric state of FADA-3210, we performed collision-induced dissociation experiments by tandem mass spectrometry (Fig. S5). For the tandem mass spectrometry measurements, the $[D]^{+12}$ and $[D]^{+11}$ dimeric charge states of FADA-3210 were selected, and the collision energy offset was varied from 15 to 100 V until the selected dimeric ions were completely dissociated. Dissociation of the precursor dimeric ions yielded the monomeric protein ions with typical asymmetric charge partitioning, in which the charge of the parent ion is unevenly distributed between the fragment ions [42,43].

Altogether, the results obtained in the mass spectrometry (MS) experiments confirm the dimeric assembly of FADA-3210 binding one dye molecule. To further corroborate these findings, we performed fluorescence activation experiments with purified protein in solution. To obtain binding equilibrium curves, we titrated purified FADA-3210 to constant concentrations of MG-2p. A 1:1 binding model to fit the experimental data cannot account for the steepness of the fluorescence activation. In contrast, a 2:1 binding model correlates well with the measured signals (Fig. S7a). Therefore, a genetic

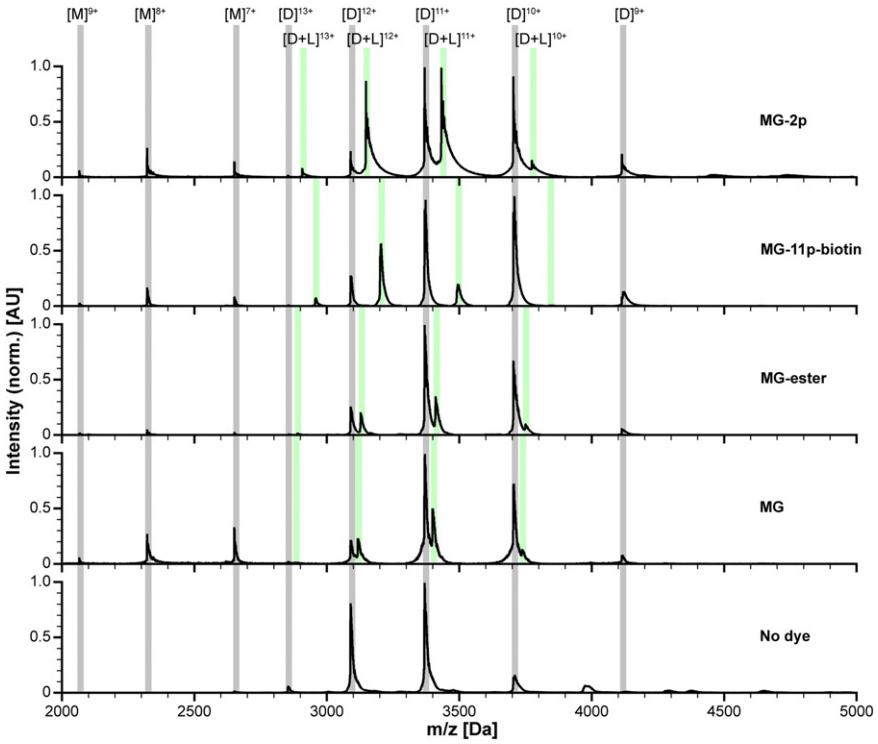

Fig. 6. Native nanoESI-MS spectra of FADA-3210. Shown are native nanoESI-MS spectra of FADA-3210 incubated either without fluorogenic dye or with different MG derivatives (MG-2p, MG-11p-biotin, MG-ester, MG). In all samples, 5 μM FADA-3210 was used and the MG dyes (termed L for ligand) were present in 5-fold excess (25 μM). The spectra show a bimodal charge state distribution with monomeric (mainly $[M]^{+9}$, $[M]^{+8}$, and $[M]^{+7}$) and dimeric charge states (mainly $[D]^{+12}$, $[D]^{+11}$, and $[D]^{+10}$) of FADA-3210 (shaded in gray). The spectra of samples incubated with MG dyes show clear peaks for dimeric FADA-3210 molecules binding one dye molecule (mainly $[D + L]^{+12}$, $[D + L]^{+11}$, and $[D + L]^{+10}$), with a shift relative to the corresponding peak of dye-free dimer, according to the different masses of the MG dyes (shaded in green). No peaks for monomeric FADA-3210 binding a dye molecule were observed.

fusion of two FADA-3210 molecules *via* a flexible linker (2×FADA-3210) was constructed, which allows intramolecular dimerization of the fused FADA-3210 molecules. This construct had identical fluorescence activation properties as FADA-3210 (Fig. S6). As expected, when titrating 2× FADA-3210 to constant concentrations of MG-2p, here a 1:1 binding model fits well to the experimental data (Fig. S7b). Together, these findings support the structural data, clearly demonstrating that FADA-3210 binds and activates MG as a homodimer in solution.

Fig. 7. FADA-3210 is a versatile reporter for fluorescence live-cell imaging. (a) Selective imaging of integral membrane proteins at the cell surface. Neurotensin receptor NTR1, parathyroid hormone 1 receptor PTH1R, or β2-adrenergic receptor β2-AR with an N-terminal 2×FADA-3210 fusion was expressed in HEK 293T cells. Cells were incubated with 200 nM MG-2p for 5 min and imaged by confocal microscopy at 633 nm excitation and 650–700 nm emission or with bright field illumination (BF). For each receptor, a strong fluorescent signal at the cell surface with little intracellular background is visible. (b) Visualization of ligand-induced receptor trafficking. 2×FADA-3210-NTR1 was expressed in HEK 293T cells, and receptors at the cell surface were stained with 200 nM MG-2p. Receptor internalization was induced by stimulation with 100 nM NT-HL488, and two-color confocal images were taken to visualize MG fluorescence (excitation, 633 nm; emission, 650–700 nm) and NT-HL488 (excitation, 488 nm; emission, 510–580 nm). NT-HL488 co-localizes with MG-2p fluorescence at the cell surface after 5 min and is internalized after 30 min together with NTR1. (c and d) Intracellular staining of cytosolic and integral membrane proteins. 2×FADA-3210-GFP or 2×FADA-3210-NTR1 was expressed in HEK 293T cells. Cells were incubated with 200 nM membrane-permeable MG-ester for 5 min to stain 2×FADA-3210-fusion proteins within the cell, and confocal images were recorded as described above. 2×FADA-3210-GFP shows an even cytosolic distribution with clear co-localization of MG-2p and GFP fluorescence. In contrast, 2×FADA-3210-NTR1 is stained at the cell surface, as well as in a perinuclear compartment, which most likely represents the Golgi apparatus.

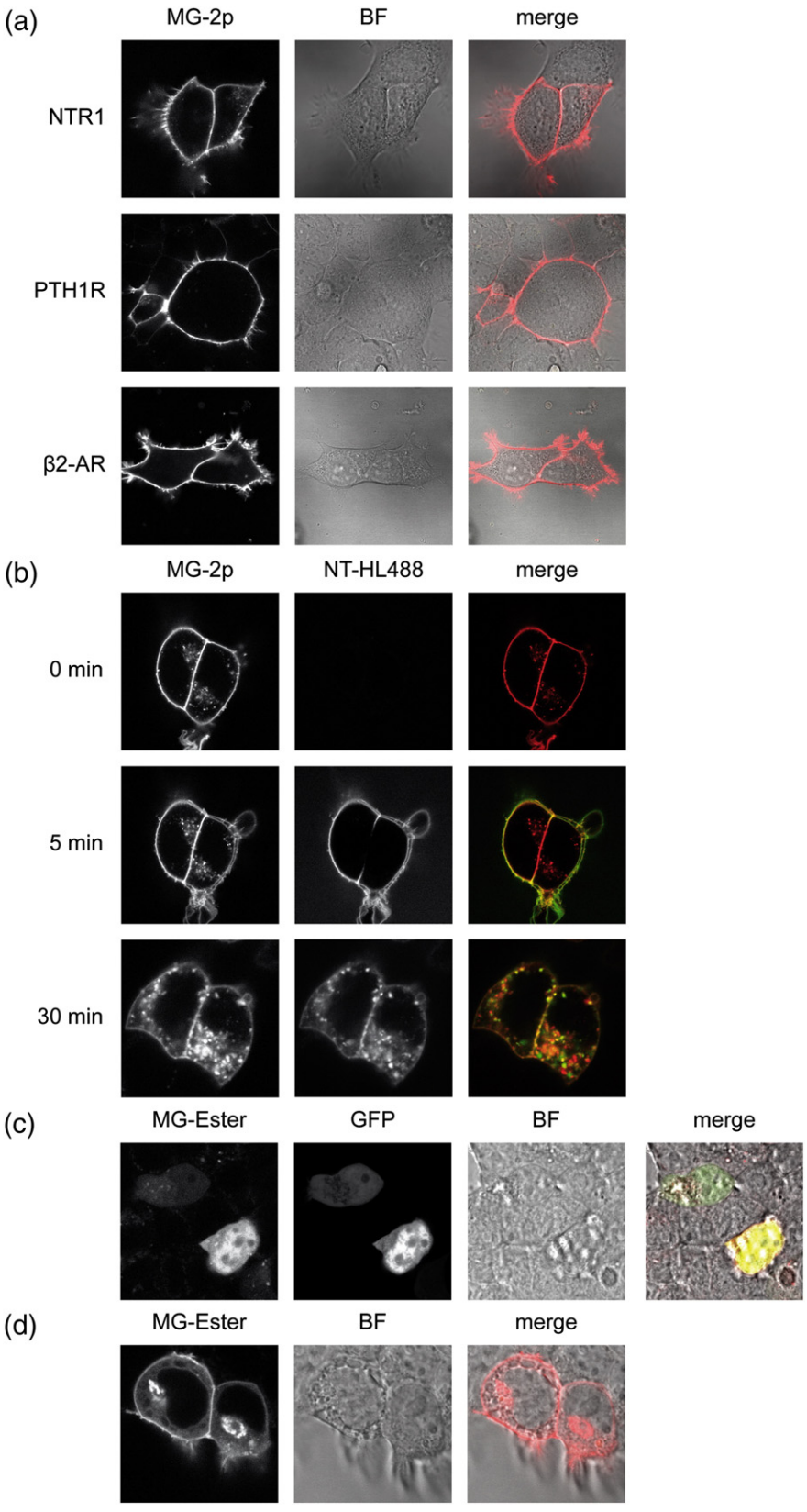

Fig. 7 (*legend on previous page*)

FADA-3210 is a versatile tool for selective labeling of proteins on the cell surface and in the cytosol

FAPs have been shown to be valuable tools for cell imaging applications as they allow homogeneous labeling of proteins with little background fluorescence. We thus explored the capabilities of FADA-3210 as a sensor for fluorescent cell imaging. For this purpose, 2×FADA-3210 was fused to the N-termini of three different G-protein-coupled receptors (2×FADA-3210-NTR1, 2×FADA-3210-PTH1R, and 2×FADA-3210-β2AR) that were then expressed in HEK 293T cells and analyzed by confocal live-cell microscopy. To selectively detect receptors on the cell surface, we incubated cells with 200 nM membrane-impermeable MG-2p, and images were taken directly after addition of the dye without any additional washing steps. For each 2×FADA-3210 receptor-fusion construct, a strong fluorescent signal was observed at the plasma membrane of transfected cells, whereas no background fluorescence was observed in untransfected cells or in the cytosol of transfected cells (Fig. 7a).

Next we assessed the versatility of the FADA sensor to monitor protein trafficking within the cell. HEK 293T cells expressing 2×FADA-3210-NTR1 were first labeled with MG-2p and then challenged with 20 nM NT-HL488 (an NTR1 agonist conjugated to a fluorescent dye) to induce receptor internalization. In the absence of ligand, a specific MG signal at the cell surface was observed, as well as in several intracellular vesicles, most likely resulting from constitutive internalization of the receptor. Addition of the ligand first resulted in co-localization of fluorescent ligand and MG at the cell surface, and after a 30-min incubation time with ligand, strong agonist-induced receptor internalization was observed with both fluorescent dyes (Fig. 7b).

In contrast to scFv-based FAPs, DARPins do not contain disulfide bonds and can thus fold equally well under non-reducing and reducing conditions such as the cytosol. We therefore analyzed the suitability of FADA-3210 for intracellular protein labeling. For this purpose, 2×FADA-3210 was fused to green fluorescent protein (GFP) and expressed in HEK 293T cells. To permit intracellular labeling, we used the membrane-permeable MG-ester. As shown in Fig. 7c, MG and GFP fluorescence co-localized well in an expression-level-dependent manner and with similar subcellular distribution, whereas almost no unspecific MG fluorescence was observed in untransfected cells. When cells expressing 2×FADA-3210-NTR1 were labeled with MG-ester, the majority of receptor was found on the cell surface. Moreover, a fraction of NTR1 resided in perinuclear patches that most likely reflect immature receptor species in the Golgi apparatus (Fig. 7d). Collectively, these data demonstrate that FADA-3210 is a versatile tag for fluorescence live-cell imaging with high specificity. Due to the unique properties of the DARPin scaffold, this tag is applicable to extracellular and intracellular targets.

Generation of a prototype biosensor by rigid DARPin-DARPin fusions with FADA-3210

Based on the results obtained from structural investigations and MS experiments, we concluded that the dimeric FADA-3210 assembly is the fluorogen-activating species. Consequently, by hindering dimerization of FADA-3210, we should prevent activation of MG-2p. When fusing a protein scaffold to FADA-3210 in such a way that, upon binding to a protein of interest, dimerization of both FADAs is blocked, this could be easily used as a fluorescent biosensor.

To investigate this concept, we created rigid fusions of FADA-3210 to another DARPin, termed 3G124, which binds GFP [28]. In these fusions, the C-terminal end of 3G124 is connected to the N-terminus of FADA-3210 by a shared rigid helix (Wu Y. *et al.*, unpublished results). Based on structural models, we generated fusions of 3G124 and FADA-3210 with two different versions of rigid DARPin-DARPin fusions (DDs), termed DD_3G124_**09**_FADA-3210 and DD_3G124_**13**_FADA-3210. These two different rigid fusions differ in the length of the shared helix and consequently in the relative orientation of the two DARPins (Fig. 8). For DD_3G124_**09**_FADA-3210, dimerization at the FADA-3210 interface (as observed in the structure of the FADA-3210 homodimer) is sterically hindered due to the orientation of the two 3G124 DARPins. In contrast, the DD_3G124_**13**_FADA-3210 construct allows dimerization in such a fashion. However, if both 3G124 DARPins bind a GFP molecule, dimerization is sterically hindered for DD_3G124_**13**_FADA-3210 as well due to the clashing of the two bound GFP molecules. Therefore, a rigid fusion of FADA-3210 in the same arrangement as in DD_3G124_**13**_FADA-3210 could serve as a prototype of a biosensor: strong MG-based fluorescence is obtained if the fusion partner DARPin to FADA-3210 is in a free state, allowing FADA-3210 to dimerize, whereas fluorescence is reduced as soon as the fusion partner DARPin binds its target. The only requirement of the target to be detected is its size, which must be sufficient to lead to a clash in the dimeric form of the biosensor upon binding. Thus, provided the target protein is large enough to meet this criterion, such a sensor would be very generic.

In order to test this concept, we performed fluorescence activation experiments in solution with purified DD**09** and DD**13** 3G124-FADA-3210 fusions (Fig. 9a). Indeed, compared to FADA-3210, fluorescence activation of DD_3G124_**09**_FADA-3210 is significantly lower, whereas DD_3G124_**13**_FADA-3210 shows identical fluorescence activation

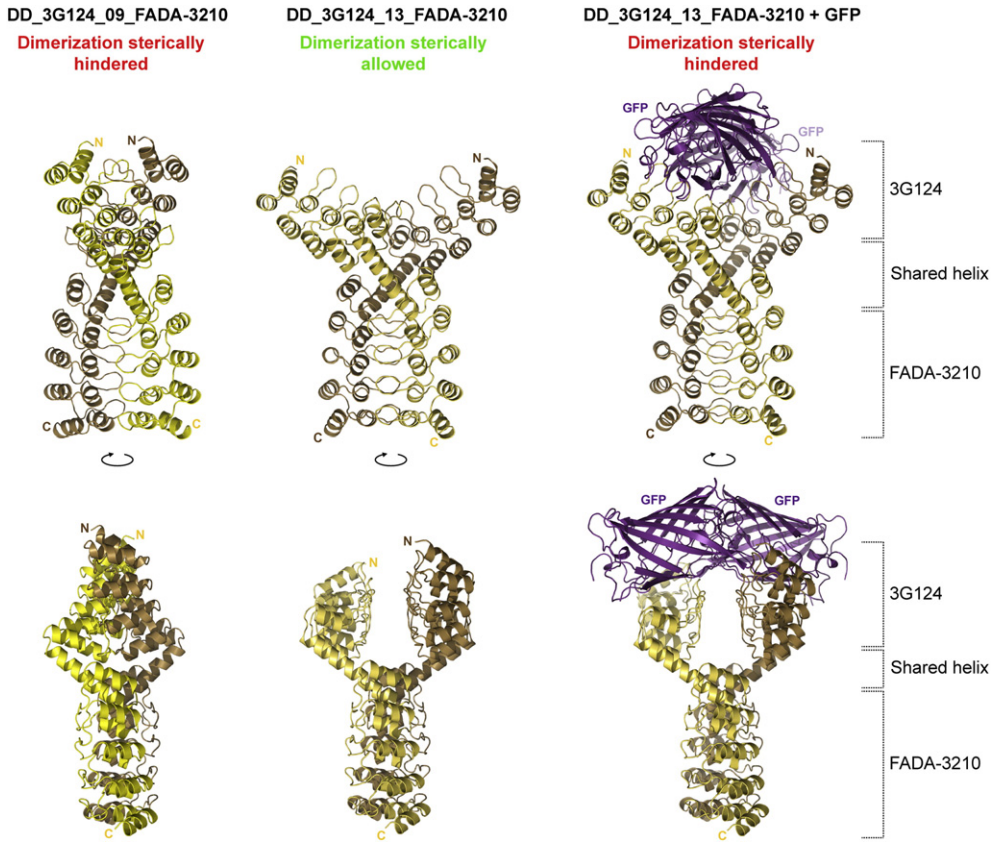

Fig. 8. Structural models of the homodimers of rigid DARPin-DARPin fusions of 3G124 and FADA-3210. Perpendicular views of structural models of homodimers of DD_3G123_**09**_FADA-3210 (left panel), DD_3G123_**13**_FADA-3210 (middle panel), and DD_3G123_**13**_FADA-3210 with bound GFP (right panel) are shown. The GFP-binding DARPin 3G124 is at the top (N-terminal), and the MG-binding DARPin FADA-3210 is at the bottom (C-terminal). The two molecules of the homodimers are depicted in yellow and brown cartoons, and the N- and C-termini of the rigid DARPin fusions are indicated (labeled with N and C, respectively). The monomers are assumed to be rigid, and the dimerization of the MG-binding DARPin orients the fusion proteins. For DD_3G123_**09**_FADA-3210, the relative orientation of the 3G124 and FADA-3210 molecules does not allow dimerization, as seen in the model of the FADA-3210 homodimer, due to clashes of the two 3G124 DARPins. Since the 3G124 and FADA-3210 DARPins have a different relative orientation in the DD_3G123_**13**_FADA-3210 fusion, dimerization is sterically allowed. However, if both 3G124 DARPins bind a GFP molecule, dimerization of DD_3G123_**13**_FADA-3210 is sterically hindered due to clashes of the GFP molecules. The models were obtained by superimposition of the C-terminal DARPin DD_**09** and DD_**13** models onto the crystal structure of the FADA-3210 homodimer. The model for DD_3G123_**13**_FADA-3210 with bound GFP was obtained by superimposition of the crystal structure of the 3G124/GFP complex (Hansen S. *et al.*, unpublished results) onto the N-terminal DARPin of the DD_3G123_**13**_FADA-3210 model.

as FADA-3210. Again, these results confirm that dimerization of FADA-3210 is responsible for the strong fluorogen activation of MG-2p observed. However, fluorogen activation is not completely lost for DD_3G124_**09**_FADA-3210 (about 80% reduced). The incomplete loss of fluorogen activation might reflect that the FADA-3210 molecules are still able to partially dimerize at the C-terminal dye-binding region even in the DD_3G124_**09**_FADA-3210 arrangement, for instance, due to bending of the connecting helix, which may not be completely rigid. Alternatively, the monomeric proteins might still contribute to fluorescence activation, albeit at a significantly reduced level. FADA-C1, however, shows only 1.6% of the fluorogen activation (Fig. 2a), suggesting that incomplete rigidity limits the performance of this first-generation prototype biosensor.

As expected from our biosensor models, we observed a reduction of fluorogen activation upon addition of GFP to DD_3G124_**13**_FADA-3210 (Fig. 9b). A 2-fold stoichiometric excess of GFP reduced the fluorescence of the unfused FAD-3210 control sample by 9%, most likely through internal filter effects. Even though such filter effects will contribute to a reduction of the fluorescence for DD_3G124_**13**_FADA-3210 as well, the observed reduction of fluorogen activation upon addition of

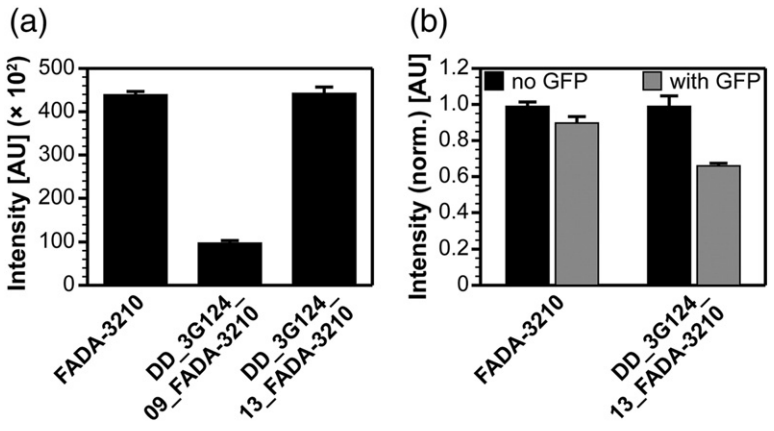

Fig. 9. Fluorescence activation assays with rigid DARPin-DARPin fusions of 3G124 and FADA-3210. (a) FADA-3210, DD_3G123_**09**_FADA-3210, or DD_3G123_**13**_FADA-3210 (always 2 μM) was incubated with 200 nM MG-2p and fluorogen activation was measured. For FADA-3210 and DD_3G123_**13**_FADA-3210, identical MG-2p activation signals are obtained. DD_3G123_**09**_FADA-3210, however, gives only about 20% fluorescence activation compared to FADA-3210 and DD_3G123_**13**_FADA-3210. Error bars indicate standard deviations of triplicates. (b) FADA-3210 or DD_3G123_**13**_FADA-3210 (100 nM) was incubated with 100 nM MG-2p in the absence (black bars) or presence (gray bars) of 200 nM GFP. Due to internal filter effects, addition of GFP slightly decreases the fluorescence activation signal obtained for FADA-3210 (9% reduction of signal). In contrast, for DD_3G123_**13**_FADA-3210, the addition of GFP leads to a significantly stronger decrease of fluorescence activation (33% reduction of signal), consistent with a steric repulsion due to bound GFP. Data were normalized to the fluorescence intensity of FADA-3210 and DD_3G123_**13**_FADA-3210 in the absence of GFP. Error bars indicate standard deviations of triplicates.

GFP was significantly larger for DD_3G124_**13**_FADA-3210 (33% reduction) than for the control sample. This shows that the sensor framework can indeed be used to detect target proteins. Nonetheless, more advanced rigid designs in future versions of the sensor will be required, since no complete loss of fluorogen activation was obtained even for the intrinsically clashing DD_3G124_**09**_FADA-3210 fusion. Also, in the present prototype, both binding sites for GFP need to be occupied. However, by increasing the rigidity and improving the geometrical arrangement, it should be feasible to create sensitive and generic sensors for protein detection in the future.

Discussion

Genetic FAP fusions have been proven to be ideally suited for the imaging of cell surface proteins [6,9,10,14] with several advantages compared to labeling of proteins by genetic fusions to fluorescent proteins or coupling to small organic fluorophores. For instance, FAP fusions in combination with cell-impermeant fluorogenic dyes allow exclusive labeling of the protein of interest on the surface with no background signal from any intracellularly residing molecules of the labeled protein [9]. In contrast, genetic fusions of fluorescent proteins to cell surface proteins inevitably lead to high intracellular background signals. Furthermore, the fluorescence of FAPs can be "turned on" or "refreshed" at any desired time point simply by addition of the fluorogenic dye, thereby allowing fluorescence imaging with spatial and temporal resolution, without being greatly affected by photobleaching. Finally, since unbound fluorogenic dyes are not fluorescent in solution, the imaging with genetic FAP fusions is highly specific and does not require any additional washing steps, which are needed in all commonly used protein or peptide tag-based fluorophore coupling systems [1–5].

In this study, we expanded the FAP technology, which so far exclusively relied on antibody scFvs, by using the DARPin scaffold to generate novel fluorogen activators termed FADAs. While DARPins previously have been selected to bind a wide variety of protein targets [18–30], we could now demonstrate that these binding proteins can be efficiently selected to bind small organic molecules as well. Compared to antibody scFvs, the DARPin scaffold provides several favorable properties, like the ease of recombinant production at high yields for instance, the very high stability, and the complete independence of intramolecular disulfide bonds for structural integrity [16,17]. Thus, the use of DARPins in many applications is straightforward and does not require any further substantial engineering steps.

Our generated FADA, termed FADA-3210, activates MG dyes to a similar extent as previously generated scFv-based FAPs with a fluorescence enhancement by a factor of more than 11,000 [6]. Interestingly, FADA-3210 forms a homodimer that encapsulates one MG-2p molecule. This mode of fluorogen activation by a dimeric arrangement of the activating protein has been previously described for two different fluorogen-activating scFvs as well [39,44]. This finding suggests that dimerization might be the key determinant for strong fluorogen activation by such binding molecules.

In fact, fluorogen activation of triarylmethane dyes, like MG, is achieved by restricting internal rotational

motion in the dye molecule and thereby preventing non-radiative relaxation by rotational de-excitation [45,46]. The bound conformation of MG in FADA-3210 is highly similar to the electronic S_0 ground state of MG [37], while the electronically excited S_1 and S_2 states relax to conformations with two rings being perpendicular and one ring in the plane of the triarylmethane center (Fig. S4). Consequently, strong fluorogen activation is obtained if the dye is held as rigidly as possible in its ground state propeller conformation, in which it remains right after electronic excitation (Franck–Condon principle) and from which a photon can be re-emitted giving rise to fluorescence. For binding proteins that provide an interaction area at the surface and not in a deep binding groove, dimerization appears to be the best solution to achieve maximal conformational restriction of a fluorogenic dye by binding it from two sides. Moreover, shielding the dye from the polar solvent environment may further contribute to maximal fluorescence activation.

Indeed, in comparison to the ancestor DARPin FADA-C1, which shows only weak fluorogen activation, FADA-3210 has only acquired five additional mutations during maturation toward strong fluorescence activation of MG-2p. None of these additional mutations makes contacts to MG-2p, but three out of five of these mutated residues are involved in dimerization contacts. Among these residues, tyrosine Y^{155} plays a key role in a strong dimerization interface. While we observed some sequence variations in different matured FADAs, Y^{155} was a strongly selected mutation and was acquired in all of the matured FADAs that showed potent fluorogen activation (data not shown). Therefore, we conclude that the maturation toward strong fluorogen activation was achieved by evolving dimerizing FADAs.

By connecting two FADA-3210 protomers with a flexible linker, we generated a fluorogenic sensor that exhibits excellent fluorescence activation properties with little background fluorescence, which can be used as a fluorescence reporter, without requiring dimerization of the fused molecule. By using the 2×FADA-3210 sensor in living cells, it was possible to detect the subcellular localization of difficult-to-express proteins such as G-protein-coupled receptors with high specificity and excellent signal-to-noise ratio. After ligand-induced endocytosis of neurotensin receptor 1, tracking of the receptor in endocytic vesicles by MG-2p fluorescence was well accomplished, demonstrating that fusion of FADAs did not largely impair protein function. Moreover, as DARPins are stable in reducing environments such as the cytosol, FADA-3210 can likewise be used as a cytosolic reporter for cytosolic proteins, as well as to stain intracellular accumulation of membrane proteins. In combination with membrane-permeable or membrane-impermeable MG derivatives, it can thus be used as reporter for specific subcellular localization of proteins. More recently, we have used this feature to construct a generic selection system for directed evolution of G-protein-coupled receptors based on the FADA technology [47].

The requirement for dimerization of FADA-3210 to obtain strong fluorescence activation of MG-2p can be used to create sensors for protein interaction or co-localization studies, by creating genetic fusions of single FADA-3210 molecules to proteins of interest. Upon addition of MG-2p, strong fluorescence would only be detectable if the proteins of interest interact and are in close proximity, allowing the single FADA-3210 molecules to form intermolecular dimers.

Furthermore, the required dimerization and the intrinsic rigidity of the DARPin scaffold allow also new sensor concepts, as we have demonstrated with a prototype of such a biosensor in this study. This prototype is based on a rigid fusion of a target-binding DARPin to FADA-3210. If the target (GFP in this study) is present, dimerization at the FADA-3210 interface is sterically hindered. Thus, addition of the target leads to a decrease of the measured fluorescence obtained from the activation of MG-2p. Due to the ease of generating DARPins specifically binding a wide variety of target molecules, we foresee the feasibility of creating target-sensing FADA molecules based on the concept of our prototype. This concept is distinct from previous biosensor applications using this scaffold, which have been based on chemically conjugated solvatochromic dyes [48–50].

Several routes are available to further improve this biosensor concept. A more rigid fusion between binding domains should further constrain the complex such that it cannot bend, a better geometric arrangement may increase sensitivity to steric clash, and the dimerization interface of FADA-3210 can be optimized to improve sensitivity.

In summary, due to the favorable properties of the DARPin scaffold and the straightforward generation of DARPins recognizing practically any target, including posttranslational modifications [26], FADAs and FADA biosensors have the potential to be widely used. Examples might include *in vivo* applications for extracellular and intracellular imaging, as well as *in vitro* detection applications, for instance, on solid matrices for chip-based sensors.

Materials and Methods

MG dyes

MG-11p-biotin, MG-2p, and MG-ester were kindly provided by Alan S. Waggoner (Carnegie Mellon University). Syntheses of these MG derivatives have been described by Waggoner and co-workers [6]. MG is commercially available and was purchased (32745, Sigma-Aldrich).

Ribosome display selections

In all ribosome display selections, the biotinylated derivative of MG, MG-11p-biotin, was used as target. The selections against MG-11p-biotin were performed using the DARPin libraries N2C and N3C as previously described [16,19,32]. Four rounds of ribosome display were carried out for each library. Round 1 was performed on NeutrAvidin-coated plates on which MG-11p-biotin was immobilized. Subsequent rounds 2–4 were carried out in solution using streptavidin-coupled magnetic beads (Dynabeads MyOne Streptavidin T1, 65602; Life Technologies). To reduce non-specific binding, we included pre-panning steps on NeutrAvidin-coated wells (round 1) and streptavidin-coupled magnetic beads (rounds 2–4). In the first round, 1 μM MG-11p-biotin was used for immobilization on NeutrAvidin-coated plates. The amount of MG-11p-biotin used was reduced to 150 nM in rounds 2–4. Washing steps were increased from round to round to minimize non-specific binding (in the first round, 35 s; in the second round, 6 min; in the third and fourth rounds, 18 min total wash time). After each round, the number of PCR cycles for amplification of selected sequences was reduced (in the first round, 40; in the second round, 35; in the third round, 30; in the fourth round, 28 PCR cycles), adjusting to the increased DNA yield due to the enrichment of binders. Enrichment of binders was only visible for the DARPin N3C pool. From the enriched DARPin N3C DNA pools, N3C DARPin open reading frames (ORFs) were amplified by PCR as previously described [32] and were ligated into the *Escherichia coli* expression vector pDST67 [23]. DARPin pools were screened by a crude-extract enzyme-linked immunosorbent assay according to previous studies [19,22]. Fifty-eight binders were identified and subjected to analytical size-exclusion chromatography. To increase the affinity of selected binders, we performed ribosome display off-rate selections as previously described [32]. Two starting pools were generated by error-prone PCR using either an equal mix of all 58 identified binders or exclusively the best behaving binders out of the 58 identified ones as DNA template. Three rounds of off-rate selections were carried out as follows: first, an enrichment round on plate was performed to remove non-binding DARPin variants (round 1). Second, the recovered DNA pool of DARPin ORFs was subjected to a selection in solution with an excess of non-biotinylated MG-2p competitor (see below) to yield highest-affinity binders (round 2). Third, a recovery round was carried out to enrich the selected high-affinity binders (round 3). The recovered N3C DARPin ORFs were subjected to a new round of error-prone PCR followed by another cycle of off-rate selections as described above (rounds 4–6). This entire cycle of mutagenic PCR and ribosome display off-rate selections was repeated one additional time (rounds 7–9). During the off-rate selections, competition with non-biotinylated MG-2p was carried out as highlighted previously [51] based on an expected affinity ranging from 50 to 150 nM of potentially affinity-maturated MG-binding DARPins. Enriched DARPin pools were subsequently cloned into the expression vector pDST67 [23] and subjected to crude-extract enzyme-linked immunosorbent assay, analytical size-exclusion chromatography, and fluorescence activation assays. From these experiments, the two MG-binding DARPins FADA-C1 and FADA-D4 were identified.

Yeast surface display

For maturation of FADA-C1 and FADA-D4 toward higher fluorogen activation, the ORFs of these two DARPins were ligated into the yeast surface display vector pCTCON2 [36] to obtain pCTCON2-FADA-C1 and pCTCON2-FADA-D4. Next, a library was created by error-prone PCR with an equal mix of these vectors leading to a randomization of the FADA-C1 and FADA-D4 sequences. The obtained DNA library was then subjected to high-efficiency transformation of the *S. cerevisiae* strain EBY100 (*MAT***a** *GAL1-AGA1*::*URA3 ura3–52 trp1 leu2Δ1 his3Δ200 pep4*::*HIS2 prb1Δ1.6R can1 GAL*) as previously described [36], giving rise to the yeast display library termed FADA 1.0. Cultivation, expression, and selection were performed as described previously [33–36]. Briefly, FADA 1.0 was subjected to selections with two rounds of FACS, in which the clones showing the highest fluorescence activation upon addition of 500 nM MG-2p (top 1.5–2.0% of the most fluorescent cells) were isolated. After FACS, the DNA of the selected pool (FADA 1.2) was isolated and subjected to another round of error-prone PCR and high-efficiency transformation, giving rise to a new yeast display library (FADA 2.0). FADA 2.0 was again subjected to two rounds of selection with FACS as described above but with a lower MG-2p concentration (100 nM MG-2p), resulting in the selected pool FADA 2.2. The whole cycle of error-prone PCR, high-efficiency transformation, and selection with two rounds of FACS was repeated for one additional time (generation of library FADA 3.0, resulting in the selected pool FADA 3.2). In order to further increase the selection stringency in this last round, we further reduced the MG-2p concentration to 50 nM in the first round and to 12.5 nM in the second round of FACS. The DNA of the selected pool (FADA 3.2) was isolated and 20 different fluorogen-activating N3C DARPins were identified by sequencing. The ORFs of the 20 selected DARPins were cloned into pCTCON2 [36] for analysis in the yeast display setup and into pDST67 [23] for expression in *E. coli*. From fluorescence activation assays performed with the 20 selected clones, the single clone FADA-3210

was identified to be the best fluorogen-activating DARPin.

Analytical flow cytometry measurements were performed on a BD FACSCanto II cytometer (BD Biosciences) and FACS was performed on a BD FACSAria III sorter (BD Biosciences). Flow cytometry and FACS data were analyzed with FlowJo (vX.0.7).

DARPin expression and purification from *E. coli*

Expression of DARPins was performed either with plasmid pDST67 [23] or with plasmid pQE30ss [derived from pQE-30 (Qiagen), containing a C-terminal double stop codon] in the *E. coli* strain XL1-Blue (200249, Agilent Technologies). For single DARPins, pre-cultures were grown in 40 mL 2×YT medium supplemented with 10 g/L glucose and 50 µg/mL ampicillin. For expression, 1 L 2×YT medium supplemented with 50 µg/mL ampicillin was inoculated from the pre-culture to OD_{600} = 0.1, growth was continued at 37 °C until the culture reached OD_{600} = 0.5–0.7, and 0.5 mM IPTG was added with subsequent cultivation at 37 °C for 5 h. Then the cultures were harvested by centrifugation, the cell pellets were re-suspended once in 25 mL cold TBS_{400} buffer [50 mM Tris–HCl (pH 7.4) at 4 °C and 400 mM NaCl] and centrifuged again, and the pellets were frozen in liquid nitrogen and stored at −80 °C until use. Expression of DD_3G124_**09**_FAD-3210 and DD_3G124_**13**_FAD-3210 constructs was performed as described above, but the temperature for the expression culture was lowered to 30 °C after addition of IPTG, and the cultivation time was increased to 16 h.

For purification, frozen cell pellets from 1 L of expression culture were thawed at room temperature and re-suspended in 30 mL lysis buffer [50 mM Tris–HCl (pH 7.4) at 4 °C, 400 mM NaCl, 20 mM imidazole, 1 mM $MgCl_2$, 1 g/L lysozyme, 2.5 mg/L DNase I, 10% (v/v) glycerol, and cOmplete ULTRA EDTA (*e*thylene*d*iamine*t*etraacetic *a*cid)-free tablets (Roche)]. The re-suspended pellets were homogenized and then ruptured by one passage through a cooled cell disrupter system at 20,000 psi. The lysates were centrifuged and the supernatant was filtered with a syringe through a Filtropur S 0.2-µM filter (Sarstedt). For immobilized metal-ion affinity chromatography, the filtered supernatant was applied to a disposable PD-10 chromatography column packed with 2–3 mL Ni-NTA Superflow resin (Qiagen) previously washed with 5 column volumes of ddH_2O and equilibrated with 15 mL TBS_{400}-W buffer [50 mM Tris–HCl (pH 7.4) at 4 °C, 400 mM NaCl, 20 mM imidazole, and 10% (v/v) glycerol]. After addition of the filtered supernatant, the immobilized metal-ion affinity chromatography columns were washed with 40 mL TBS_{400}-W buffer and the protein was eluted with 0.5–1.5 mL TBS_{400}-E buffer [50 mM Tris–HCl (pH 7.4) at 4 °C, 400 mM NaCl, 250 mM imidazole, and 10% (v/v) glycerol]. Eluted purified protein was frozen in liquid nitrogen and stored at −80 °C until use.

Fluorescence activation assays in solution

Fluorescence activation assays in solution were performed in FADA assay buffer [10 mM Tris–HCl (pH 7.4) at 4 °C, 150 mM NaCl, 2 mM EDTA, and 0.1% (w/v) Pluronic F-127] at 4 °C. Purified FADAs were applied to PD-10 desalting columns (GE Healthcare) for a buffer exchange to FADA assay buffer. Subsequently, the FADAs were mixed with MG dyes in FADA assay buffer and incubated for at least 20 min on ice without exposure to light. Fluorescence activation was then measured in a 96-well black microplate (655209, Greiner Bio-One) on an Infinite M1000 plate reader (Tecan) with an excitation wavelength of 630 nm and a measured emission wavelength of 645 nm.

For measurements of excitation and emission spectra, either the excitation wavelength was scanned from 490 to 690 nm in steps of 5 nm with a constant measured emission at 700 nm (excitation scan) or the measured emission wavelength was scanned from 590 to 790 nm in steps of 5 nm with a constant excitation wavelength of 580 nm (emission scan).

Fluorescence activation assays with DD_3G124_**09**_FAD-3210 and DD_3G124_**13**_FAD-3210 constructs were performed as described above with the exception that purified GFP (in FADA assay buffer) was added to the incubation mixture wherever stated.

X-ray crystallography

Purified FADA-3210 was thawed on ice and the buffer was exchanged to HBS [10 mM HEPES (pH 7.4) and 150 mM NaCl] using PD-10 desalting columns (GE Healthcare). The protein was concentrated to 20–25 mg/L using an Amicon Ultra centrifugal filter unit with a 10-kDa molecular weight cutoff (EMD Millipore). Solid MG-2p was added to the protein solution at a 2:1 dye-to-protein molar ratio and mixed. Undissolved MG-2p was removed by a brief centrifugation before setting up the crystallization experiments. Crystallization was performed in crystalQuick crystallization plates (Greiner Bio-One) by sitting-drop vapor diffusion at 20 °C. The FADA-3210/MG-2p solution was mixed with the mother liquor at 1:1, 1:2, and 2:1 ratios for each condition tested. Crystals of FADA-3210 in complex with MG-2p were obtained in 20% (w/v) polyethylene glycol 3350 and 0.2 M sodium malonate (pH 5.0). The obtained crystals appeared as thin green-colored plates (Fig. S8) and were mounted directly from the mother liquor on CryoLoops (Hampton Research) and frozen in liquid nitrogen.

X-ray diffraction data were collected using the PILATUS 2M high-resolution detector at 1.0 Å wavelength on the beamline X06DA at the Swiss Light Source (Paul Scherrer Institut) from a single protein crystal cryo-cooled to 100 K. The crystal belonged to space group $P12_11$ with 12 FADA-3210 molecules in the asymmetric unit. Diffraction data were processed and scaled using the program XDS [52]. Resolution of the data was cut at 2.6 Å with $I/\sigma(I) = 0.86$ and $CC_{1/2} = 0.55$ [53].

The structure was determined by molecular replacement with Phaser [54] and the off7 DARPin structure (PDB ID: 1svx) as a search model. The search model was prepared by removing all non-protein atoms and the maltose binding protein from the off7 DARPin structure. Model building was performed using Coot [55] and refinement was performed with REFMAC5 [56] and phenix.refine [57]. Data collection and refinement statistics calculated with PHENIX graphical tools [58] are shown in Table S1.

Mass spectrometry

Purified FADA-3210 was thawed at room temperature and the buffer was exchanged to 100 mM ammonium acetate (pH 6.9) using PD-10 desalting columns (GE Healthcare). All MS measurements were performed with 5 μM FADA-3210 in 100 mM ammonium acetate (pH 6.9).

Electrospray ionization analyses were performed with a Q-TOF Ultima hybrid quadrupole time-of-flight mass spectrometer (Waters/Micromass). Calibration of the MS instrument was performed with cesium iodide clusters. Cesium iodide was dissolved in a 1:1 mixture of Optima liquid chromatography/MS water (Fisher Chemical) and liquid chromatography/MS CHROMASOLV 2-propanol (Sigma-Aldrich) at a concentration of 2 μg/mL. Ions were formed using nanoflow platinum-coated borosilicate electrospray capillaries (Proxeon). For all nanoESI-MS measurements, the capillary voltage was optimized between 0.9 and 1.2 kV and a gentle backing pressure of 0.3–0.5 bar was applied to assist the liquid sample flow. The source temperature was kept at 30 °C. The mass spectrometer was run with the following parameters for gentle desolvation: the cone and first ion tunnel RF1 voltages, parameters that control the kinetic energy of the ions in the source region of the mass spectrometer, were set to 80 V and 60 V, respectively. After this stage, the ion beam passed a hexapole collision cell filled with 5.0-purity argon (PanGas). The collision energy offset was used to optimize desolvation and set to 30 V. The pressure in the analyzer region (pressure of argon in the collision cell) was adjusted to 1.1×10^{-4} mbar and the time-of-flight pressure was 7.47×10^{-7} mbar. The ion transmission was optimized for an m/z range from 1000 to 8000 Da. The following mass range settings of the quadrupole were used: 2000 Da (lower m/z), 3000 Da (peak m/z transmission), and 8000 Da (upper m/z). Optimized dwell time settings were used to maximize the intensity of the ion m/z range within a scan by dwelling on the appropriate quad MS profile. The scan time and interscan times were 1 s and 0.1 s, respectively. Before data processing, each mass spectrum was smoothed (Savitzky–Golay filter [59]) with the MassLynx 4.0 software (Waters). To identify the component in the mass spectra, we performed analysis by using the transform algorithm of the MassLynx 4.0 software.

2×FADA-3210 expression constructs for life cell imaging

For N-terminal 2×FADA-3210 receptor-fusion constructs, the signal sequence of 5-HT_{3a} serotonin receptor (MRLCIPQVLLALFLSMLTGPGEGS) followed by a Flag tag (DYKDDDDK) was fused to the 5′ end of 2×FADA-3210 by PCR and inserted into pcDNA5/FRT (V6010-20, Thermo Fisher Scientific). The coding sequences of rat neurotensin receptor NTR1, human parathyroid hormone 1 receptor PTH1R, or human β2-adrenergic receptor β2-AR were then inserted directly after the 2×FADA-3210 cassette, resulting in 2×FADA-3210-NTR1, 2×FADA-3210-PTH1R, and 2×FADA-3210-β2-AR, respectively. The 2×FADA-3210-GFP expression construct was constructed by introducing 2×FADA-3210 into pEGFP-N1 (6085-1, Clontech) at the 5′ end of EGFP.

Live-cell imaging

HEK 293T/17 cells (American Type Culture Collection) were maintained in Dulbecco's modified Eagle's medium (D6429, Sigma) supplemented with 10% (v/v) fetal calf serum and 100 μg/mL of penicillin and 100 μg/mL of streptomycin in a 5% CO_2 atmosphere. For transient transfections, cells were seeded on 18-mm coverslips and transfected with 2×FADA-3210-fusion constructs using TransIT-293 (Mirus). At 48 h after transfection, coverslips were mounted in an imaging chamber, and cells were washed once and maintained in Tyrode buffer [137 mM NaCl, 5.4 mM KCl, 2 mM $CaCl_2$, 1 mM $MgCl_2$, and 10 mM Hepes (pH 7.3)] at 37 °C. For labeling of FADA-3210, we added 200 nM MG-2p or 200 nM MG-ester to the buffer solution and incubated it for 5 min. Co-staining and internalization of NTR1 was achieved by adding 20 nM neurotensin (8–13) conjugated to HiLyte Fluor 488 (NT-HL488, synthesized by AnaSpec/Eurogentec) to the MG labeling solution. Confocal images were taken at indicated time points on a Leica TCS SP5 laser scanning microscope using single-line excitation at 488 nm and 633 nm and an emission bandwidth of 510–580 nm and 650–700 nm for MG and HiLyte Fluor 488 fluorescence, respectively.

Protein Data Bank accession code

The atomic coordinates of the FADA-3210/MG-2p complex structure were deposited in the Protein Data Bank (PDB ID: 5aao).

Acknowledgements

We thank Claudia Dumrese, Cornelius Fischer, Vinko Tosevski, and Florian Mair (Flow Cytometry Facility) for support with FACS; Beat Blattmann and Céline Stutz-Ducommun (Protein Crystallization Center) for support with protein crystallization; the staff from beamlines X06SA and X06DA from the Swiss Light Source (Paul Scherrer Institute, Villigen, Switzerland) for support during X-ray data collection; and Annemarie Honegger for helpful comments and input on construction of rigid DARPin-DARPin fusions. C.K. was supported by a fellowship of the German Academy of Sciences Leopoldina (LPDS 2009-48) and a Marie Curie fellowship of the European Commission (FP7-PEOPLE-2011-IEF #299208). G.A.N was supported by a Fulbright Scholarship. This work was funded by European Research Council Advanced Grant NEXTBINDERS and Schweizerischer Nationalfonds grant 31003A_146278 (both to A.P.).

Author Contributions: M.S., A.B., and C.K. contributed equally to this work; M.S., L.K., and A.P. designed the project; M.S., L.K., S.d.P., G.A.N., and E.S. performed selections; M.S., Y.W., and J.S. performed protein characterization and fluorescence activation experiments; A.B. and Y.W. conducted protein expression, purification, and crystallization; A.B. and P.R.E.M. determined the structure; A.B. designed the rigid FADA sensor prototypes; C.K. performed *in vivo* labeling experiments and microscopy; B.G. carried out MS experiments; F.Z. developed the quantitative binding model; M.S., C.K., B.G., and A.P. analyzed the data; R.Z., K.D.W., and A.P. supervised the project; M.S., C.K., and A.P. wrote the manuscript with the help of all authors.

Conflict of Interests: The authors declare no conflict of interests.

Appendix A. Supplementary data

Supplementary data to this article can be found online at http://dx.doi.org/10.1016/j.jmb.2016.01.017.

Received 2 December 2015;
Received in revised form 12 January 2016;
Accepted 15 January 2016
Available online 23 January 2016

Keywords:
protein engineering;
directed evolution;
fluorogen-activating proteins;
designed ankyrin repeat proteins;
biosensors

Present address: M. Schütz and L. Kummer, G7 Therapeutics AG, Grabenstrasse 11a, CH-8952 Schlieren, Switzerland.

Present address: B. Gülbakan, Institute of Child Health, Hacettepe University, 06100 Ankara, Turkey.

Present address: G. A. Newby, Whitehead Institute for Biomedical Research, Cambridge, MA 02142, USA.

Present address: E. Sedlák, Centre for Interdisciplinary Biosciences and Department of Biochemistry, Pavol Jozef Šafárik University in Košice, 040 01 Košice, Slovakia.

Abbreviations used:
DARPin, designed ankyrin repeat protein; nanoESI-MS, nanoelectrospray ionization mass spectrometry; MS, mass spectrometry; FACS, fluorescence-activated cell sorting; FAP, fluorogen-activating protein; GFP, green fluorescent protein; MG, malachite green; scFv, single-chain variable fragment; ORF, open reading frame.

References

[1] B.A. Griffin, S.R. Adams, R.Y. Tsien, Specific covalent labeling of recombinant protein molecules inside live cells, Science 281 (1998) 269–272.
[2] A. Keppler, S. Gendreizig, T. Gronemeyer, H. Pick, H. Vogel, K. Johnsson, A general method for the covalent labeling of fusion proteins with small molecules *in vivo*, Nat. Biotechnol. 21 (2003) 86–89.
[3] N. George, H. Pick, H. Vogel, N. Johnsson, K. Johnsson, Specific labeling of cell surface proteins with chemically diverse compounds, J. Am. Chem. Soc. 126 (2004) 8896–8897.
[4] I. Chen, M. Howarth, W. Lin, A.Y. Ting, Site-specific labeling of cell surface proteins with biophysical probes using biotin ligase, Nat. Methods 2 (2005) 99–104.
[5] G.V. Los, L.P. Encell, M.G. McDougall, D.D. Hartzell, N. Karassina, C. Zimprich, et al., HaloTag: A novel protein labeling technology for cell imaging and protein analysis, ACS Chem. Biol. 3 (2008) 373–382.
[6] C. Szent-Gyorgyi, B.F. Schmidt, B.A. Schmidt, Y. Creeger, G.W. Fisher, K.L. Zakel, et al., Fluorogen-activating single-chain antibodies for imaging cell surface proteins, Nat. Biotechnol. 26 (2008) 235–240.
[7] H. Özhalici-Ünal, C.L. Pow, S.A. Marks, L.D. Jesper, G.L. Silva, N.I. Shank, et al., A rainbow of fluoromodules: A promiscuous scFv protein binds to and activates a diverse set of fluorogenic cyanine dyes, J. Am. Chem. Soc. 130 (2008) 12620–12621.
[8] N.I. Shank, K.J. Zanotti, F. Lanni, P.B. Berget, B.A. Armitage, Enhanced photostability of genetically encodable fluoromodules based on fluorogenic cyanine dyes and a promiscuous protein partner, J. Am. Chem. Soc. 131 (2009) 12960–12969.

[9] G.W. Fisher, S.A. Adler, M.H. Fuhrman, A.S. Waggoner, M.P. Bruchez, J.W. Jarvik, Detection and quantification of beta2AR internalization in living cells using FAP-based biosensor technology, J. Biomol. Screen. 15 (2010) 703–709.
[10] J. Holleran, D. Brown, M.H. Fuhrman, S.A. Adler, G.W. Fisher, J.W. Jarvik, Fluorogen-activating proteins as biosensors of cell-surface proteins in living cells, Cytometry A 77 (2010) 776–782.
[11] K.J. Zanotti, G.L. Silva, Y. Creeger, K.L. Robertson, A.S. Waggoner, P.B. Berget, et al., Blue fluorescent dye–protein complexes based on fluorogenic cyanine dyes and single chain antibody fragments, Org. Biomol. Chem. 9 (2011) 1012–1020.
[12] M.J. Saunders, C. Szent-Gyorgyi, G.W. Fisher, J.W. Jarvik, M.P. Bruchez, A.S. Waggoner, Fluorogen activating proteins in flow cytometry for the study of surface molecules and receptors, Methods 57 (2012) 308–317.
[13] M.J. Saunders, W. Liu, C. Szent-Gyorgyi, Y. Wen, Z. Drennen, A.S. Waggoner, et al., Engineering fluorogen activating proteins into self-assembling materials, Bioconjug. Chem. 24 (2013) 803–810.
[14] G.W. Fisher, M.H. Fuhrman, S.A. Adler, C. Szent-Gyorgyi, A.S. Waggoner, J.W. Jarvik, Self-checking cell-based assays for GPCR desensitization and resensitization, J. Biomol. Screen. 19 (2014) 1220–1226.
[15] A. Wörn, A. Plückthun, Stability engineering of antibody single-chain Fv fragments, J. Mol. Biol. 305 (2001) 989–1010.
[16] H.K. Binz, M.T. Stumpp, P. Forrer, P. Amstutz, A. Plückthun, Designing repeat proteins: Well-expressed, soluble and stable proteins from combinatorial libraries of consensus ankyrin repeat proteins, J. Mol. Biol. 332 (2003) 489–503.
[17] A. Kohl, H.K. Binz, P. Forrer, M.T. Stumpp, A. Plückthun, M.G. Grütter, Designed to be stable: Crystal structure of a consensus ankyrin repeat protein, Proc. Natl. Acad. Sci. U. S. A. 100 (2003) 1700–1705.
[18] A. Plückthun, Designed ankyrin repeat proteins (DARPins): Binding proteins for research, diagnostics, and therapy, Annu. Rev. Pharmacol. Toxicol. 55 (2015) 489–511.
[19] H.K. Binz, P. Amstutz, A. Kohl, M.T. Stumpp, C. Briand, P. Forrer, et al., High-affinity binders selected from designed ankyrin repeat protein libraries, Nat. Biotechnol. 22 (2004) 575–582.
[20] P. Amstutz, H.K. Binz, P. Parizek, M.T. Stumpp, A. Kohl, M.G. Grütter, et al., Intracellular kinase inhibitors selected from combinatorial libraries of designed ankyrin repeat proteins, J. Biol. Chem. 280 (2005) 24715–24722.
[21] D. Steiner, P. Forrer, M.T. Stumpp, A. Plückthun, Signal sequences directing cotranslational translocation expand the range of proteins amenable to phage display, Nat. Biotechnol. 24 (2006) 823–831.
[22] C. Zahnd, F. Pecorari, N. Straumann, E. Wyler, A. Plückthun, Selection and characterization of Her2 binding-designed ankyrin repeat proteins, J. Biol. Chem. 281 (2006) 35167–35175.
[23] D. Steiner, P. Forrer, A. Plückthun, Efficient selection of DARPins with sub-nanomolar affinities using SRP phage display, J. Mol. Biol. 382 (2008) 1211–1227.
[24] J. Winkler, P. Martin-Killias, A. Plückthun, U. Zangemeister-Wittke, EpCAM-targeted delivery of nanocomplexed siRNA to tumor cells with designed ankyrin repeat proteins, Mol. Cancer Ther. 8 (2009) 2674–2683.
[25] N. Stefan, P. Martin-Killias, S. Wyss-Stoeckle, A. Honegger, U. Zangemeister-Wittke, A. Plückthun, DARPins recognizing the tumor-associated antigen EpCAM selected by phage and ribosome display and engineered for multivalency, J. Mol. Biol. 413 (2011) 826–843.
[26] L. Kummer, P. Parizek, P. Rube, B. Millgramm, A. Prinz, P.R.E. Mittl, et al., Structural and functional analysis of phosphorylation-specific binders of the kinase ERK from designed ankyrin repeat protein libraries, Proc. Natl. Acad. Sci. U. S. A. 109 (2012) E2248–E2257.
[27] P. Parizek, L. Kummer, P. Rube, A. Prinz, F.W. Herberg, A. Plückthun, Designed ankyrin repeat proteins (DARPins) as novel isoform-specific intracellular inhibitors of c-Jun N-terminal kinases, ACS Chem. Biol. 7 (2012) 1356–1366.
[28] M. Brauchle, S. Hansen, E. Caussinus, A. Lenard, A. Ochoa-Espinosa, O. Scholz, et al., Protein interference applications in cellular and developmental biology using DARPins that recognize GFP and mCherry, Biol. Open 3 (2014) 1252–1261.
[29] J. Schilling, J. Schöppe, E. Sauer, A. Plückthun, Co-crystallization with conformation-specific designed ankyrin repeat proteins explains the conformational flexibility of BCL-W, J. Mol. Biol. 426 (2014) 2346–2362.
[30] O. Scholz, S. Hansen, A. Plückthun, G-quadruplexes are specifically recognized and distinguished by selected designed ankyrin repeat proteins, Nucleic Acids Res. 42 (2014) 9182–9194.
[31] H.K. Binz, P. Amstutz, A. Plückthun, Engineering novel binding proteins from nonimmunoglobulin domains, Nat. Biotechnol. 23 (2005) 1257–1268.
[32] B. Dreier, A. Plückthun, Rapid selection of high-affinity binders using ribosome display, Methods Mol. Biol. 805 (2012) 261–286.
[33] E.T. Boder, K.D. Wittrup, Yeast surface display for directed evolution of protein expression, affinity, and stability, Methods Enzymol. 328 (2000) 430–444.
[34] D.W. Colby, B.A. Kellogg, C.P. Graff, Y.A. Yeung, J.S. Swers, K.D. Wittrup, Engineering antibody affinity by yeast surface display, Methods Enzymol. 388 (2004) 348–358.
[35] G. Chao, W.L. Lau, B.J. Hackel, S.L. Sazinsky, S.M. Lippow, K.D. Wittrup, Isolating and engineering human antibodies using yeast surface display, Nat. Protoc. 1 (2006) 755–768.
[36] J.A. Van Deventer, K.D. Wittrup, Yeast surface display for antibody isolation: Library construction, library screening, and affinity maturation, Methods Mol. Biol. 1131 (2014) 151–181.
[37] A. Nakayama, T. Taketsugu, Ultrafast nonradiative decay of electronically excited states of malachite green: *Ab initio* calculations, J. Phys. Chem. A 115 (2011) 8808–8815.
[38] C. Baugh, D. Grate, C. Wilson, 2.8 Å crystal structure of the malachite green aptamer, J. Mol. Biol. 301 (2000) 117–128.
[39] C. Szent-Gyorgyi, R.L. Stanfield, S. Andreko, A. Dempsey, M. Ahmed, S. Capek, et al., Malachite green mediates homodimerization of antibody VL domains to form a fluorescent ternary complex with singular symmetric interfaces, J. Mol. Biol. 425 (2013) 4595–4613.
[40] J.A. Loo, Studying noncovalent protein complexes by electrospray ionization mass spectrometry, Mass Spectrom. Rev. 16 (1997) 1–23.
[41] J.M. Daniel, S.D. Friess, S. Rajagopalan, S. Wendt, R. Zenobi, Quantitative determination of noncovalent binding interactions using soft ionization mass spectrometry, Int. J. Mass Spectrom. 216 (2002) 1–27.
[42] J.C. Jurchen, E.R. Williams, Origin of asymmetric charge partitioning in the dissociation of gas-phase protein homodimers, J. Am. Chem. Soc. 125 (2003) 2817–2826.
[43] J.C. Jurchen, D.E. Garcia, E.R. Williams, Further studies on the origins of asymmetric charge partitioning in protein homodimers, J. Am. Soc. Mass Spectrom. 15 (2004) 1408–1415.

[44] N. Senutovitch, R.L. Stanfield, S. Bhattacharyya, G.S. Rule, I.A. Wilson, B.A. Armitage, et al., A variable light domain fluorogen activating protein homodimerizes to activate dimethylindole red, Biochemistry 51 (2012) 2471–2485.
[45] G. Oster, Y. Nishijima, Fluorescence and internal rotation: Their dependence on viscosity of the medium 1, J. Am. Chem. Soc. 78 (1956) 1581–1584.
[46] M.S. Baptista, G.L. Indig, Effect of BSA binding on photophysical and photochemical properties of triarylmethane dyes, J. Phys. Chem. B 102 (1998) 4678–4688.
[47] C. Klenk, J. Ehrenmann, M. Schütz, A. Plückthun, A generic selection system for improved expression and thermostability of G protein-coupled receptors by directed evolution, Sci. Rep. (2016) in press.
[48] E. Brient-Litzler, A. Plückthun, H. Bedouelle, Knowledge-based design of reagentless fluorescent biosensors from a designed ankyrin repeat protein, Protein Eng. Des. Sel. 23 (2010) 229–241.
[49] F.F. Miranda, E. Brient-Litzler, N. Zidane, F. Pecorari, H. Bedouelle, Reagentless fluorescent biosensors from artificial families of antigen binding proteins, Biosens. Bioelectron. 26 (2011) 4184–4190.
[50] L. Kummer, C.-W. Hsu, O. Dagliyan, C. MacNevin, M. Kaufholz, B. Zimmermann, et al., Knowledge-based design of a biosensor to quantify localized ERK activation in living cells, Chem. Biol. 20 (2013) 847–856.
[51] C. Zahnd, C.A. Sarkar, A. Plückthun, Computational analysis of off-rate selection experiments to optimize affinity maturation by directed evolution, Protein Eng. Des. Sel. 23 (2010) 175–184.
[52] W. Kabsch, XDS, Acta Crystallogr. D Biol. Crystallogr. 66 (2010) 125–132.
[53] P.A. Karplus, K. Diederichs, Linking crystallographic model and data quality, Science 336 (2012) 1030–1033.
[54] A.J. McCoy, R.W. Grosse-Kunstleve, P.D. Adams, M.D. Winn, L.C. Storoni, R.J. Read, Phaser crystallographic software, J. Appl. Crystallogr. 40 (2007) 658–674.
[55] P. Emsley, B. Lohkamp, W.G. Scott, K. Cowtan, Features and development of Coot, Acta Crystallogr. D Biol. Crystallogr. 66 (2010) 486–501.
[56] G.N. Murshudov, P. Skubák, A.A. Lebedev, N.S. Pannu, R.A. Steiner, R.A. Nicholls, et al., REFMAC5 for the refinement of macromolecular crystal structures, Acta Crystallogr. D Biol. Crystallogr. 67 (2011) 355–367.
[57] P.V. Afonine, R.W. Grosse-Kunstleve, N. Echols, J.J. Headd, N.W. Moriarty, M. Mustyakimov, et al., Towards automated crystallographic structure refinement with phenix.refine, Acta Crystallogr. D Biol. Crystallogr. 68 (2012) 352–367.
[58] N. Echols, R.W. Grosse-Kunstleve, P.V. Afonine, G. Bunkóczi, V.B. Chen, J.J. Headd, et al., Graphical tools for macromolecular crystallography in PHENIX, J. Appl. Crystallogr. 45 (2012) 581–586.
[59] A. Savitzky, M.J.E. Golay, Smoothing and differentiation of data by simplified least squares procedures, Anal. Chem. 36 (1964) 1627–1639.
[60] R.A. Laskowski, M.B. Swindells, LigPlot+: Multiple ligand–protein interaction diagrams for drug discovery, J. Chem. Inf. Model. 51 (2011) 2778–2786.